Egyptian Journal of Aquatic Biology & Fisheries
Zoology Department, Faculty of Science,
Ain Shams University, Cairo, Egypt.
ISSN 1110 – 6131
Vol. 29(4): 51– 72 (2025)
www.ejabf.journals.ekb.eg

Self-Assembly Preparation of α-FeOOH Nanorods on Natural Diatomite and Its Application in the Remediation of Cu(II)

Dalia R. AbdEl-Hafiz[1], Wessam E. Rasmy[1], Dina M. Ali[2]*

[1]Egyptian Petroleum Research Institute, Nasr City, Cairo, Egypt
[2]Botany Department, Faculty of Science, Ain Shams University, Cairo, Egypt

***Corresponding Author:** dinamohamedali12@sci.asu.edu.eg

ARTICLE INFO

Article History:
Received: May 8, 2025
Accepted: June 30, 2025
Online:

Keywords:
Adsorption,
Chemisorption,
Diatomite,
FeOOH,
Self-assembly

ABSTRACT

A novel α-FeOOH nanorods decorated hierarchically porous diatomite (FeOOH/Di) was prepared by the self-assembling method to be used in water treatment processes. The structure and surface property of the prepared nanocomposite was characterized by X-ray diffraction (XRD), Brunauer-Emmett-Teller (BET) analysis, and scanning electron microscopy images (SEM). The adsorption of Di with the prepared FeOOH/Di was applied for effective Cu^{2+} adsorption from aqueous solution. Adsorption with FeOOH/Di was reached faster and more efficiently (60min and 100% removal efficiency) than parent diatomite (120min with 54% removal efficiency). Different adsorption conditions as contact time, initial Cu^{2+} concentration and temperature were tested. The adsorption capacities increase with an increase in the initial concentration of the copper with a maximum adsorption capacity of Di and Di/FeOOH with 99.41mg g-1 at 130ppm and 164.46mg g^{-1} at 100ppm initial Cu^{2+} concentration, respectively. The removal efficiency increased with an increase in adsorption temperature up to 100ºC.The α-FeOOH/Di nanocomposites presented excellent performance of both highly reactive surface hydroxyl sites and hierarchically porous silica consisting of large surface area and huge porous volume. Kinetic, thermodynamic and adsorption isotherm were investigated. The adsorption over parent Di was found to be physisorption process on homogenous surface, while, that over FeOOH/Di was chemisorptions process on heterogeneous adsorbent surface. Thermodynamic data show highly negative ΔG value and highly positive ΔH and ΔS, indicating that, the adsorption process is a spontaneous, disordered and endothermic process, confirming the improvement of the adsorption process after decorating the Di with FeOOH molecules.

INTRODUCTION

Water pollution by heavy metals with high specific gravity (< 5) and high atomic weight (63–200) has long been considered an important environmental concern owing to their toxic properties. These elements pose huge environmental dangers for the health of the human body **(Srivastava & Majumder 2008)**. Researchers worldwide have been

encouraged to solve this problem. Different techniques have been used to extract heavy metals from industrial wastewater, including membrane filtration flocculation, adsorption, precipitation, electrolytic removal, ion exchange, reduction and reverse osmosis **(Sharma *et al.*, 2009; Moghaddam & Naimi-Jamal, 2018;Yadav *et al.*, 2019; Chai *et al.*, 2020; Ghasemi *et al.*, 2020, 2021)**. Among these techniques, adsorption is well known as a flexible and cost-effective method **(Mashhadzadeh *et al.*, 2018; Yang *et al.*, 2018)**. Therefore, it is widely used in the industrial sector **(Alomar *et al.*, 2017; Homayoon *et al.*, 2017)**. Adsorption is a cost-effective, fast, environmentally safe, and easy process, and the adsorbent can be reused several times without performance deterioration **(Gusain *et al.*, 2020)**. To clearly discuss adsorption processes, the fundamental concept of adsorption must be understood. **Dabrowski (2001)** define the adsorption isotherm, which is the main fundamental concept, as the equilibrium between the adsorbed quantity and the concentration in the bulk. Moreover, thermodynamics and kinetics are important factors that can help understand the adsorption process. Therefore, in this study, the mechanisms and thermodynamics of Cu over diatomite were investigated using a series of batch studies. The effectiveness of the adsorption for removal of heavy metal depends on the diffusion of adsorbate ions into the solid surface. In addition, the adsorbate can form bonds with the solid surface or be held by weak intermolecular forces **(De Castro Dantas *et al.*, 2001)**. Therefore, it is necessary to search for materials that can control these two factors and obey the legislation of heavy metal content in water **(Fernández-Luqueño *et al.*, 2013)**. Different adsorbent with different structure and with a variety of active sites are used for water purification, include metal oxide and/or metal supported high surface area material **(Choma, 2011; Chua, 2015)** such as biomass **(Vakili *et al.*, 2014)**, high surface area silica **(Atta *et al.*, 2016)** chitosan **(Maity & Ray, 2018)**, and hierarchical carbon **(Koduru *et al.*, 2019)**. Among these adsorbents, the OH groups on the surface of magnetic iron nanoparticles provide a platform for the attachment of various functionalities **(Lin *et al.*, 2015)**. Recently, a considerable attention was given to the applications of nanostructured metal oxides and modified graphene for the adsorption of heavy metals from aqueous solution **(Wu *et al.*, 2019; Valenzuela *et al.*, 2021; Lemessa *et al.*, 2023)**. Goethite (α-FeOOH) is a natural mineral in soils/sediments that is widely used in water treatment as a low-cost and highly reactive adsorbent **(Faria *et al.*, 2014; Maia *et al.*, 2019; Xie *et al.*, 2020; Zhang *et al.*, 2021)**. However, this reactivity decreases rapidly owing to the aggregation of FeOOH nanoparticles; therefore, it is necessary to use suitable supports to stabilize the nanoscale of the FeOOH adsorbent **(Yang *et al.*, 2018)**.

Diatomite is siliceous sedimentary rock, light in color with chalk-like appearance, very fine-grained, with low thermal conductivity and a rather high fusion point. Diatomite is essentially formed from the cell walls of fossilized ruminants. It is composed of amorphous silica ($SiO_2 \cdot nH_2O$) and a small amount of microcrystalline material **(Ilia *et al.*, 2009; Ghobara *et al.*, 2024)**. Diatom frustules are naturally considered sources of

nanomaterials. Cell wall of diatoms frustules are formed of rigid amorphous silica which have a unique porous architecture and high surface area **(Wang *et al.*, 2013)**. Recently, they have been used in many applications, including water filtration membranes, lithium battery electrodes, gas sensors, electroluminescent display devices, dye-sensitized solar cells, biochips, and drug delivery **(Thakkar & Mitra, 2017; Hamed, 2023)**. Diatomite has been successfully used for adsorption owing to their small particle size, large surface area, high porosity, high permeability, and low thermal conductivity **(ElSayed, 2018)**. In addition, the high abundance of silicon hydroxyl groups on the diatomite surface allows it to support various metal oxides and serves as potential adsorption sites for heavy metal ions **(Song *et al.*, 2022)**.

Many researches focused on the incorporation of ferric oxide on natural diatomite. **Jang *et al.* (2007)** successfully prepared hydrous ferric oxide incorporated into diatomite. **Xiong and Peng (2008)** reported the effective adsorbent of phosphorus by prepared ferrihydrite-modified diatomite. **Knoerr *et al.* (2013)** prepared iron oxide modified diatomite, by an environmentally friendly process and recorded its higher sorption capacity of As (III) from solution. **Du *et al.* (2022)** used two types of nanostructured Fe-Mn oxide composites grown *in situ* on the surface of diatomite and sepiolite for the adsorption removal of arsenic ions. They found that FeOOH-MnO_2/Sepiolite and Fe_2O_3-MnO_2/Diatomite adsorbents exhibited excellent performance for the adsorption of As(V) in wastewater. **Wang *et al.* (2021)** prepare magnetic diatomites with Fe0/iron oxide nanoparticles and recorded its highly efficient adsorbent for recovering phosphorus from water. **Luo *et al.* (2023)** stated that ferrous sulfide supported on modified diatomite (FeS/DT) has a maximum adsorption capacity for Cr(VI).

This work aimed to develop and use natural products such as diatomite as a support for the stabilization of FeOOH nanoparticles, to make it more effective for heavy metal removal from industrial water. Low-cost and selective FeOOH/diatomite nanoparticles were prepared by the self-assembly method and characterized using different analytical techniques: XRD, FTIR, BET, and SEM. It is attempted to be an innovative technique to use diatomite as a support for FeOOH, either in heavy metal adsorption or in other applications. The objectives of this study were to improve the adsorption process under different conditions: temperature, time, and initial concentration. The adsorption fundamentals like: isotherms, kinetics and thermodynamics of the adsorption process were also studied.

MATERIALS AND METHODS

Diatomite

The diatomite sample used in this study was collected from Dimai, located to the west of El-Fayoum Depression. The diatomaceous earth deposits are chalky, generally soft, light-weight, fine-grained, ranging in color from grayish white to white with brownish shades. These samples were related to the early to middle Holocene.

Pretreatment of diatomite

For this purpose, an amount of diatomite was ground to powder using a mechanical mixing grinder with a mesh size of ~200nm, and then calcined at 200˚C with acid mixture for 2h to remove organic components according to **Jousé *et al.* (1969)**, followed by cleaning and mounting according to **Taylor *et al.* (2005)**.

Self-assembling of FeOOH on diatomite surface

5g of the treated diatomite silica was suspended in 500ml of deionized water and then sonicated for 1h. After that, an appropriate amount of $FeCl_3.6H_2O$ was added into the suspension to get 10 wt% Fe/diatomite. Subsequently, the mixture was subjected to ultra-sonication for 1h and refluxed at 90^oC for 4h. The prepared sample was then centrifuged, washed and dried at 80^oC for 4h.

Characterizations of the prepared samples

The counting of the identified algae was determined by using the method described by **Vilbaste (1994)**.

Shimadzu XD-1 diffractometer with Cu-target and Ni-filtered radiation was used to analyze X-ray diffraction (XRD). N_2 adsorption–desorption isotherms (BET) and textural properties were measured at the liquid nitrogen temperature (-196^oC) using a NOVA2000 gas sorption analyzer (Quanta Chrome Corporation) system. The BET surface area (S_{BET}) was calculated using the five-point Brunauer–Emmett–Teller (BET) theory.

Scanning electron microscopy (SEM) of the diatomite sample aimed to reveal the structure and architecture of diatoms cell wall, and their predicted role in adsorption. The samples were prepared for SEM according to the method of **Hasle and Fryxell (1970)**. Additionally, transmission electron microscopy (TEM) was carried out using a JEOL 2100F TEM at an accelerating voltage of 200 kV.

Adsorption experiments

The adsorption of Cu^{2+} on the prepared samples was performed by batch adsorption experiments. Standard solution (1000ppm) of $CuCl_2$ was prepared and then diluted to the required concentrations (25-250^oC). 10ml of $CuCl_2$ solution was shaked at 400rpm using a Velp Scientifica shaker for different contact time (0- 250min). The adsorption temperature was adjusted at 25- 100^oC. The solution was filtered at the end of the experiment.

Then, the remaining amount of Cu^{2+} was measured using a spectrophotometric technique (UNICO 4802 UV/Vis double beam). The copper concentration was determined at 620nm using an ammonia solution as the reagent. The results were expressed in terms of removal efficiency (%) and adsorption capacity (mg g^{-1}), according to the following relationships:

$$\text{Removal efficiency (\%)} = \frac{C_0 - C_e}{C_0} \times 100 \qquad (1)$$

$$\text{Adsorption capacity} \left(\frac{mg}{g}\right) = \frac{C_0 - C_e}{m} \times V \qquad (2)$$

Where, C_0 and Ce are the initial and final concentrations, respectively, m is the mass of adsorbent (mg), and V is the volume of copper solution (L).

RESULTS AND DISCUSSION

Diatom diversity

As shown in Table (1), a total of ten genera and twenty-seven species were identified. Based on the analysis of the diatomite sample, the most common species were *Epithemia turgida*, *E. sorex*, *Rhopalodia gibba*, *R. gibba* var. *ventricosa*, *R. musculus*, *R. vermicularis*, and *Aulacoseira granulata*, followed by *Cocconeis placentula* and *C. placentula* var. *euglypta*. This was confirmed by the relative abundance of diatoms across all stations (Fig. 1).

Table 1. The mean frequencies of diatoms species from the collected sample

Taxa		Taxa	
Genus: *Amphora* Ehrenberg		**Genus:*Aulacoseira* Thwaites**	
***Amphora coffeiformis* (Ag.) Kütz**	+	*Aulacoseira granulata* (Ehr.) Simonsen	c
***A. ovalis*Kütz.**	+	*A. granulata* var. *angustissima* (O.F. Müller) Simonsen	r
Genus: *Campylodiscus* Ehrenberg		**Genus: *Cocconeis* Ehrenberg**	
***Campylodiscus clypeus* Ehr.**	r	*Cocconeis placentula* Ehr.	f
Genus: *Cyclotella* Kützing		*C. placentula* var.*euglypta* (Ehr.) Cl.	f
***Cyclotella meneghiniana*Kütz.**	r	**Genus: *Cymatopleura* W.Smith**	
***C. ocellata* Pant.**	r	*Cymatopleuraelliptica* (Bréb.) W.Sm.	+
Genus: *Cymbella* Agardh		*C. solea* (Bréb.) W.Sm.	r
***Cymbella affinis*Kütz.**	c	**Genus:*Epithemia* de Brébisson**	
***C. laencelata* (Ehr.) V. H.**	c	*Epithemia adanta*(Kütz.)Bréb	+
***C. minuta* Hilse**	r	*E. sorex* Kütz.	p
***C. turgida* (Greg.) Cl.**	r	*E. turgida* (Ehr.) Kütz.	p
***C. tumida* (Bréb.) V. H.**	c	**Genus:*Rhopalodia* O. Müller**	
***C.ventricosa* (Kütz.)**	r	*Rhopalodia gibba* (Ehr.) O.Müller	f
***Genus: Navicula* Bory**		*R..gibba* var. *ventricosa* (Ehr.) O.Müller.	f
***Navicula cryptocephala* Kütz.**	+	*R.. musculus*(Kütz.) O.Müll.	f
***N. cuspidata* (Kütz.) Cl.**	+	*R.. vermicularis* O.Müll.	c
***N. radiosa* Kütz.**	+		

p= predominant (50-20%), f= frequent (20-5%), c= common (5-1%), r= rare (1-0.2%), += noted

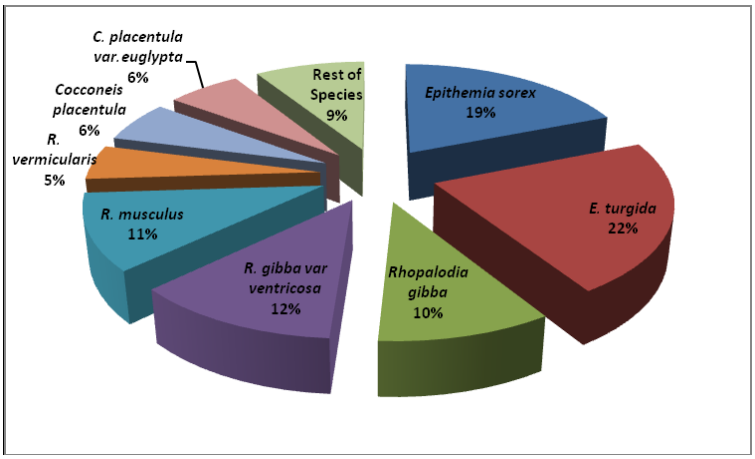

Fig. 1. Percentage of the most common species identified from the diatomite sample (total no. of individuals counted /200 valve)

Cocconeis placentula var. euglypta, C. placentula, Epithemia sorex, E. turgida, Rhopalodia vermicularis, R. gibba var. ventricosa, and *Aulacoseira granulata* are typically heavily silicified and robust. Their valves exhibit thickened internal costae **(Kingston, 2003; Lowe, 2003; Wolin & Stone, 2010)**. These species are the most predominant in the diatomite deposits collected from Dimai, located west of the El-Fayoum Depression.

Scanning electron microscopy (SEM) of *Epithemia turgida* (Fig. 2a–c) revealed a strongly silicified cell wall architecture, characterized by dense costae running across the frustule and high porosity. The striae are spaced at 8–10 per 10µm, while the costae are 4–5 per 10µm, with 2–3 striae present between each costa. SEM analysis of *Aulacoseira granulata* (Fig. 2d) showed dense silicification of the mantle, featuring numerous square-shaped areolae, also in the range of 8–10 per 10µm.

Transmission electron microscopy (TEM) images of both the unmodified (parent) diatoms and FeOOH-functionalized diatoms are presented in Fig. (3a, b). Fig. (3a) illustrates the parent diatoms exhibiting hierarchically interconnected pore structures. In contrast, Fig. (3b) shows FeOOH uniformly anchored onto the diatom surface, forming rod-like bundles that are approximately 30nm in length and ~1 nm in diameter. These TEM images confirm that the FeOOH/diatom composite displays a nanorod-decorated hierarchical porous structure, which is advantageous for Cu^{2+} adsorption due to its abundance of active adsorption sites and enhanced mass transfer properties **(Fu *et al.*, 2017)**.

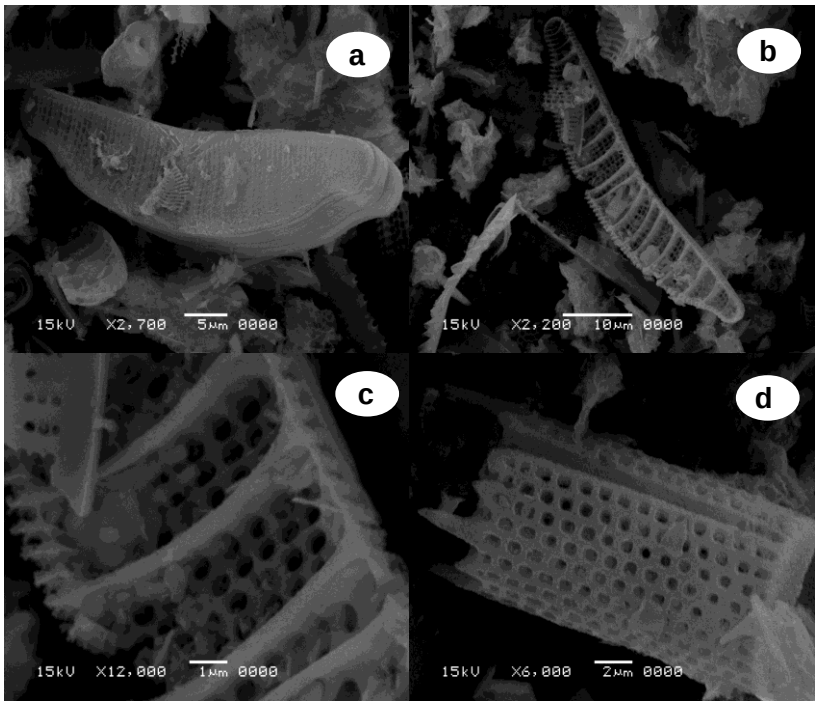

Fig. 2. (a-c). *Epithemia turgida* (SEM) a. External view of the upper and central part of the valve exhibiting external fissure and areola. b. Internal view of the valve. c. Internal view of the central part of the valve exhibiting internal raphe canal and continuous coastae. d. *Aulacoseira granulata* cylindrical mantle wall perforated by distinct areolae, which are varied in shape from rounded to quadrate. Scale bars: see in each figure

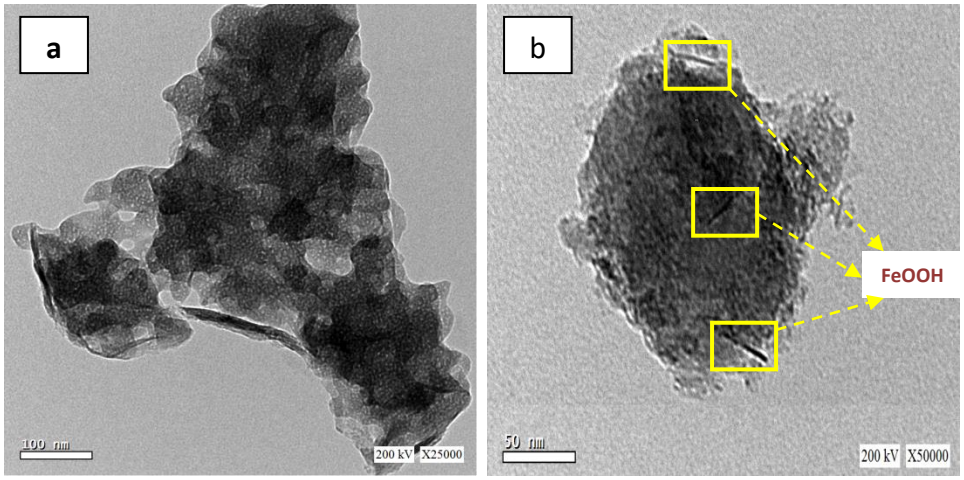

Fig. 3. TEM image of: a) parent diatoms b) FeOOH/diatoms

XRD diffraction pattern of the parent diatomite shows an amorphous structure (Fig. 4). Four diffraction peaks were observed for the FeOOH/Di sample at 2θ = 35.17, 39.95, 55.71 and 63.19º (JCPDS 13-87) indicating the formation of α-FeOOH with planes of 100, 002, 102, and 110 **(Maia *et al.*, 2019)**. The presence of the amorphous phase observed at 2θ 4o to 24° is due to the glass formation of SiO2 **(Nenadovic *et al.*, 2015)**. The N_2 adsorption/desorption isotherms of the prepared FeOO/H/diatoms (Fig. 5) show a type IV isotherm with a relevant microporous contribution **(Lucchini *et al.*, 2016)**.

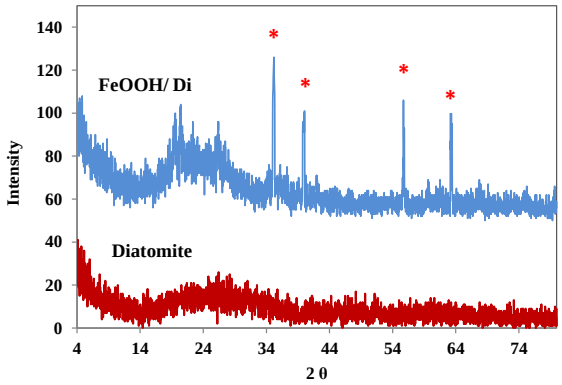

Fig. 4. XRD pattern of the prepared parantdiatomes and FeOOH/Di

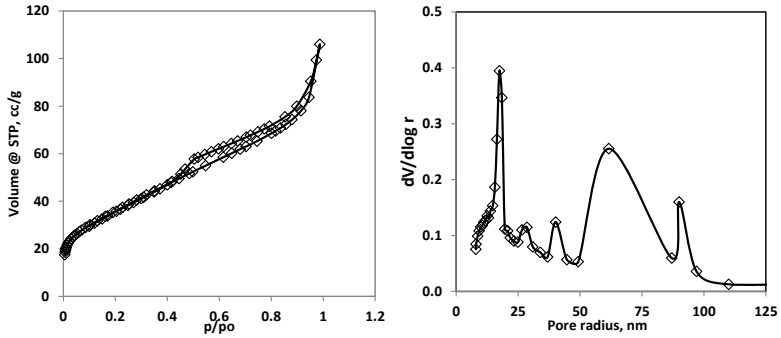

Fig. 5. Texture properties of the prepared FeOOH/Diatoms

According to the IUBC classification, the IV isotherm characteristics corresponded to mesoporous and macroporous materials **(Fu *et al.*, 2017)**. The dramatic increase of the isotherm also refers to the contribution of macropores **(Lu *et al.*, 2020)**.

The hysteresis loop is H3 type indicating a slit- shaped, layered structure of disordered form and size consistent with SEM and TEM data. Moreover, a multipore size distribution was observed in the BJH pattern within the radius range from 15- 100nm. This indicates that the hierarchical porous structure ranges from micro- to macropores **(Lu *et al.*, 2020)**. Therefore, the prepared FeOOH/Diatoms (SBET = 130 m2 g-1) can be used as an efficient adsorbent; because it not only permits solutes to adsorb onto the outer surface but also guarantees diffusion through the interconnecting micro- and mesoporous channels and binds the adsorption sites on the inner surface **(Liu *et al.*, 2019)**. The average pore size of FeOOH/Diatoms is larger than Cu2+ diameters (0.256 nm), so it can exhibit special adsorption performance towards cupper.

Batch adsorption experiments

Adsorption kinetics

The adsorption experiment was conducted on both samples at room temperature varying the contact time from 0 to 250min, and the initial Cu^{2+} solution concentration was fixed at 100ppm. As shown in Fig. (6), the adsorption was very fast initially due to the high number of available sites at the initial stage, then gradually slowed down until reaching the adsorption equilibrium (qe).

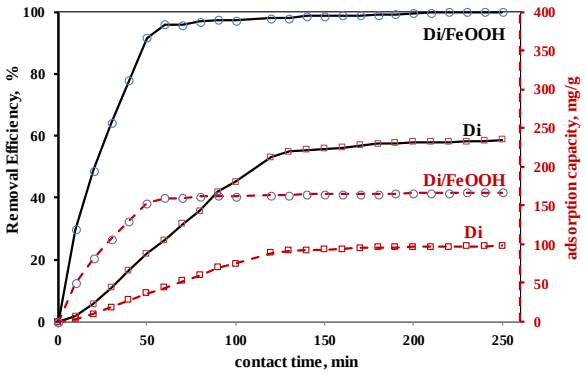

Fig. 6. Contact time effect on Cu2+ removal efficiency and diatomite adsorption capacity at 298K, 100ppm initial concentration and 0.6 gL-1 adsorbent mass

The adsorption over parent diatomite reached the adsorption equilibrium (88.49mg g^{-1}) within 120min with 54% removal efficiency, while over FeOOH/Di the adsorption equilibrium (159.82mg g^{-1}) reached more quickly (within 60min) with 100% removal efficiency.

The kinetics of Cu^{2+} adsorption on diatomite earth and FeOOH decorated diatomite were studied to describe the controlling mechanism of adsorption for both samples. The kinetics data are shown in Fig. (7). Pseudo-first-order (Eqn. 3), pseudo-second-order (Eqn. 4), and the intraparticle diffusion (Weber-Morris diffusion model) equations were used to study the adsorption kinetics.

$$\text{Pseudo} - \text{first} - \text{order}: \quad \log(q_e - q_t) = \log q_e - \frac{k_1}{2.303} t \tag{3}$$

$$\text{pseudo} - \text{second} - \text{order}: \quad \frac{t}{q_t} = \frac{1}{k_2 q_e^2} + \frac{1}{q_e} \tag{4}$$

$$\text{initial rate of adsorption}: \quad h = k_2 q_e^2 \tag{5}$$

$$\text{Weber} - \text{Morris diffusion}: \quad q_t = k_{id} t^{1/2} + C \tag{6}$$

Where, q_t and q_e are the amounts of Cu^{2+} adsorbed (mg g^{-1}) at time t (min) and at equilibrium, respectively. k_1 (min^{-1}) and k_2 (g mg^{-1} min^{-1}) are the rate constant for first-order and second-order, respectively. h is the initial rate of adsorption (mg g^{-1} h). Moreover, K_{id} (g mg^{-1} h) is the intraparticle diffusion rate constant.

According to the experimental results, (Table 2 & Fig. 7), the parent Di adsorbent follows the pseudo-first-order kinetic model (R^2 = 0.979), indicating that physical adsorption is the rate-determining step. This physical adsorption is a result of the electrostatic attraction between the Cu^{2+} cation and the external surface of the Di adsorbent. On the other hand, the pseudo-second-order model is more suitable (R^2 = 0.996) for estimating adsorption kinetics over FeOOH/Di adsorbent, suggesting a chemical adsorption nature.

Additionally, the initial rate of adsorption (h) of Cu2+ over FeOOH/Di was significantly higher than that over the parent Di. The increased adsorption of Cu2+over FeOOH/Di sample is attributed to the chemical bond formed between Cu2+and surface FeOOH functional groups in addition to the electrostatic attraction between the external diatomite surface **(Hakami *et al.*, 2012)**.

Table 2. Kinetic data for adsorption process over both Di and Di/FeOOH

	t_e, min	$q_{e,exp}$ mg g^{-1}	Pseudo-first-order model			Pseudo-second-order model				Weber-Morris diffusionmodel		
			K_1 min^{-1}	$q_{e,cal}$ mg g^{-1}	R^2	K_2 min^{-1}	$q_{e,cal}$ mg g^{-1}	R^2	h mg g^{-1} h	K_{id} g mg^{-1} h	C	R^2
Di	120	91.59	$-25x10^{-3}$	128.09	0.98	$2.3x10^{-5}$	196.08	0.77	0.896	11.032	-38.81	0.9797
FeOOH/Di	60	159.8	$-23x10^{-3}$	65.27	0.87	$5x10^{-3}$	178.57	0.99	178.57	26.213	-34.911	0.9979

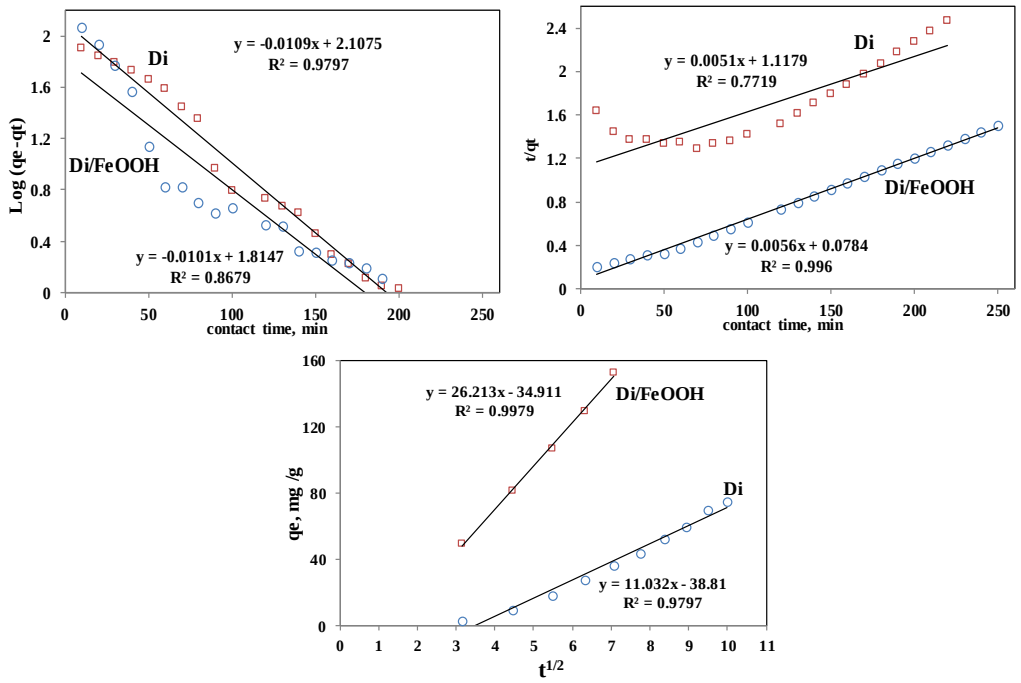

Fig. 7. Adsorption Kinetic plots of Cu2+ over both Di and Di/FeOOH

This is supported by the control of this adsorption reaction by a second-order mechanism, where, the surface FeOOH functional groups act as chelators forming an inner-sphere surface complex with Cu2+ **(Fu *et al.*, 2017; Maia *et al.*, 2019)**, as shown in scheme (1). This synergistic effect greatly enhances the adsorption performance of the prepared FeOOH/Di as a promising adsorbent for Cu^{2+}removal from solution.

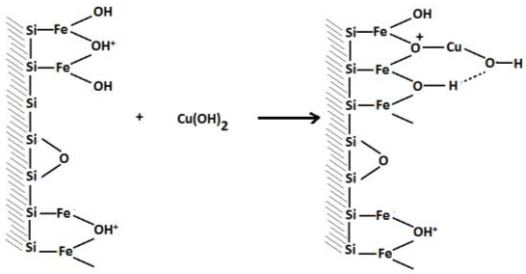

Scheme (1). Schematic diagram of inner-sphere surface complex formation of Cu2+ with FeOOH as chelators

It is known that any adsorption process is governed by the rate of three diffusion steps of adsorbed molecules from the aqueous solution to the adsorbent surface. These steps included diffusion from the aqueous phase to the adsorbent interface, diffusion from the interface to the adsorbent surface (intraparticle diffusion), and the movement of the adsorbate into the adsorbent pores (coordination adsorption). To analyze the rate-controlling step of adsorption, the intraparticle diffusion (Weber-Morris diffusion model) equation was utilized **(Zeng *et al.*, 2015)**.

The data in Fig. (7) show that the intraparticle diffusion models do not pass through the origin, confirming that this stage not only controls the adsorption mechanism, but also that there are other mechanisms that can influence Cu^{2+} adsorption over both Di and FeOOH/Di.

Effect of initial concentration

The effects of changing initial Cu2+ concentrations on the adsorption behavior of both Di and Di/FeOOH are illustrated in Fig. (8). Data indicate that the adsorption capacities of Cu2+ over Di increase with an increase in the initial concentration of the copper solution due to the enhancement of metal ions mass transfer **(Wang *et al.*, 2013)**, then reaches a plateau at 130 ppm, with a maximum adsorption capacity of approximately 99.41mg g-1.

On the other hand, using Di/FeOOH as an adsorbent shows a maximum adsorption capacity of 164.46mg g^{-1} at 100ppm initial Cu^{2+} concentration.

The experimental studies also showed that the removal efficiency was inversely proportional to the initial metal concentrations. Where 100% removal was observed at 50ppm over Di/FeOOH adsorbent. The decrease in removal efficiency may be attributed to the number of adsorption sites available that are not enough, which requires a higher amount of adsorbent to achieve higher removal.

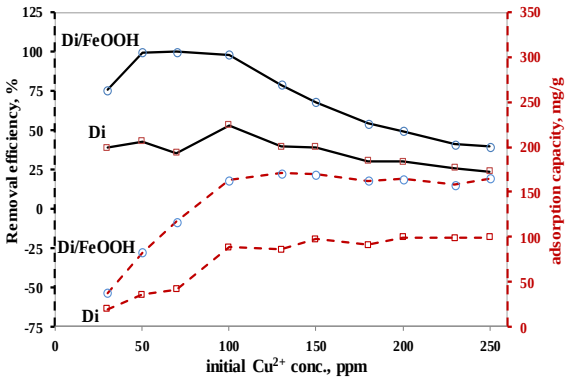

Fig. 8. Initial Cu2+ concentration effect on Cu2+ removal efficiency and diatomite adsorption capacity, at 298 K, 120min contact time and 0.6 gL-1 adsorbent mass

Adsorption isotherm

The BET (Eqn. 7), Freundlich (Eqn. 8) and Langmuir (Eqn. 9) models were used to study the relationship between the Cu^{2+} ions during adsorption onto Di and FeOOH/Di surface.

BET equation: $$\frac{C_e}{(C_s-C_e)q_e} = \frac{1}{BQ^o} + \left(\frac{B-1}{BQ^o}\right)\frac{C_e}{C_s} \quad (7)$$

Fruendlich equation: $$\log q_e = logK + \frac{1}{n}\log C_e \quad (8)$$

$$\text{Langmuir equation:} \quad \frac{C_e}{q_e} = \frac{1}{K} + \frac{a}{K} C_e \tag{9}$$

$$R_L = \frac{1}{1 + K_L C_o} \tag{10}$$

Where, Cs and Ce are the initial and equilibrium concentration (ppm); qe is the adsorption capacity at equilibrium (mg g^{-1}); B, Q^o, K, a are constants; n is the adsorption intensity; and R_L is the Langmuir separation factor.

The adsorption isotherm data are illustrated in Fig. (9) and listed in Table (3). The obtained (n) values calculated from the Freundlich isotherm model were found to be 1.54 and 7.24mg g-1 for Di and FeOOH/Di, respectively. These values fall within the range of 1 < n < 10 which is favorable for the adsorption process. Additionally, higher values of R2 were found to be 0.8 and 0.98 for Di and FeOOH/Di, respectively, indicating the applicability of the Langmuir model of adsorption compared to other models. The fitting of the Langmuir model of the isotherm suggests that the adsorption occurs on a homogeneous surface with all adsorption sites having equal adsorption affinity **(Hao *et al.*, 2010)**.

The Langmuir separation factor was found to be within the range of 0 < RL< 1, indicating that the adsorption is favorable for both samples. It is closer to 0 for the FeOOH/Di sample suggesting an irreversible adsorption process **(Singh *et al.*, 2015)**.

Table 3. Adsorption isotherm data for both Di and Di/FeOOH

	BET equation			**Fruendlich**			**Langmuir**			
	R^2	**B**	**Q^o**	**R^2**	**K_F**	**n**	**R^2**	**K_L**	**A**	**R_L (at C^o:30-50 ppm)**
Di	0.015	3.02	23.98	0.23	4.16	1.54	0.8	1.76	0.011	0.0186 - 0.0023
FeOOH/Di	0.74	70.5	70.92	0.79	83.16	7.24	0.98	39.53	0.233	0.0008 - 0.0001

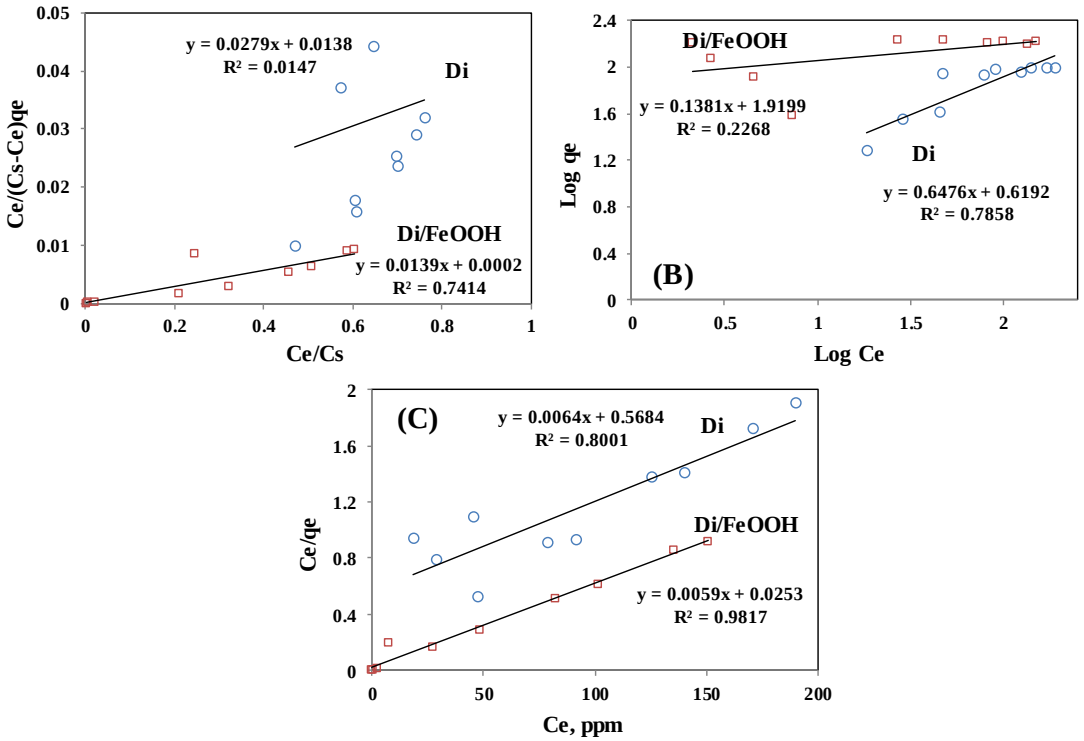

Fig. 9. Adsorption isotherm plots of Cu2+ adsorption over both Di and Di/FeOOH
A. BET model B. Fruendlichmodel C. Langmuir model

Effect of adsorption temperature

The effects of changing adsorption temperature on the adsorption behavior of both Di and Di/FeOOH are illustrated in Fig.(10). The adsorption temperature changed from 20 to 100ºC.

Dara depicted in Fig. (10) indicate that the removal efficiency increased with rising adsorption temperature, becoming more favorable up to 100°C. This improvement is attributed to the greater number of molecules gaining sufficient energy to interact with active sites on the surface **(Todorciuc *et al.*, 2015)**.

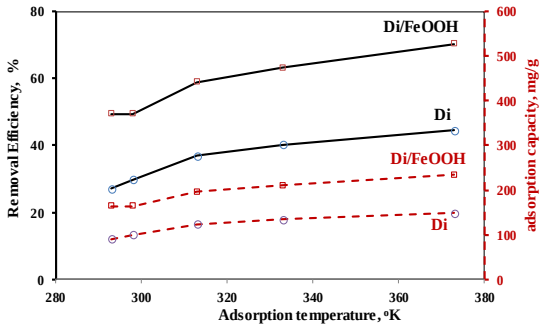

Fig. 10. Adsorption temperature effect on Cu2+ removal efficiency and diatomite adsorption capacity, at 200ppm, 120min contact time and 0.6 gL-1 adsorbent mass

Thermodynamic study

Thermodynamics parameter: Gibbs free energy change (ΔG), standard enthalpy change (ΔH) and the standard entropy change (ΔS) were calculated (Eqn. 9 - 12) at temperatures ranging from 293 – 373 K to determine the feasibility, spontaneity and heat change of Cu2+ adsorption over both Di and FeOOH/Di **(Atar & Olgun, 2009; Yadav *et al.*, 2014)**.

$$K_d = \frac{q_e}{C_e} \quad (9)$$

$$LnK_d = \frac{\Delta S}{R} - \frac{\Delta H}{RT} \quad (10)$$

$$\Delta G = -RT\ LnK_d \quad (11)$$

$$\Delta G = \Delta H - T\,\Delta S \quad (12)$$

Where, K_d is the distribution coefficient for Cu^{2+} between liquid and solid at equilibrium; R is the universal gas constant; J mol^{-1} K, T is the absolute temperature in Kelvin.

The calculated thermodynamic data are listed in Table (4). The negative ΔG values confirm the spontaneous nature of Cu2+ adsorption over both samples. It is known that, 0 < ΔG< 20 kJ mole-1indicates a physical adsorption process, while ΔG> 20kJ mole-1indicates a chemical adsorption process **(Yu *et al.*, 2001)**.

Table 4. Thermodynamic data for adsorption of Cu2+ using Di and Di/FeOOHas adsorbent

T, Kelvin	Di			FeOOH/Di		
	ΔG J mol^{-1}	ΔH J mol^{-1}	ΔS J $mol^{-1}K^{-1}$	ΔG J mol^{-1}	ΔH J mol^{-1}	ΔS J $mol^{-1}K^{-1}$
293	-20555	8432	44.79	-27813	10500	59.09
298	-20779			-28108		
313	-21451			-28994		
333	-22347			-30176		
373	-23138			-32540		

In this study, the ΔG values in Table (4) indicate the physisorption nature of Cu2+ adsorption over Di, while the chemisorption nature of Cu2+ adsorption over FeOOH/Di is confirmed by the kinetic study. The positive ΔH values indicate the endothermic nature of adsorption. This can be explained by what is known as the solvent replacement theory **(Zeng *et al.*, 2015)**. The hydrogen bond formed between the adsorbent and water molecules when the adsorbent is added to the aqueous solution. For adsorption to occur, those water molecules must first desorb from the adsorbent surface.

Thus, more heat is needed for the water desorption process, and overall Cu2+ adsorption over Di and FeOOH/Di was endothermic. Additionally, the ΔH <84 kJ/mole for adsorption over Di confirms the physisorption process, and ΔH ≈ 105kJ/mole confirms the chemisorption process **(Faust & Aly, 1987)**.

Furthermore, the ΔS values were calculated to understand the degree of disorder in the adsorption system. A high degree of disorder in the system improves the adsorption thermodynamically and makes the process more favorable. In this study, the ΔS has positive values, indicating the disordered system of adsorption. Moreover, the system of Cu^{2+} adsorption over FeOOH/Di (59.09 J $mol^{-1}K^{-1}$) was more disordered than that over Di (44.79 J $mol^{-1}K^{-1}$), confirming the improvement of the adsorption process after decorating the Di with FeOOH molecules. These high entropy values may be attributed to the increase in degrees of freedom during the water molecules desorption process to form bonds between Cu^{2+} and the adsorbent system.

CONCLUSION

FeOOH nanoroads were self-assembled on the surface of a hierarchically porous diatomite structure and used as an adsorbent. The structure and surface properties of the prepared sample were confirmed by different analytical techniques: XRD, BET, TEM and SEM. FeOOH/Di showed more efficient adsorption of Cu^{2+} from aqueous solutions than the parent diatom. This can be attributed to the fact that the assembly of FeOOH on the diatom surface increases the active adsorption sites in addition to the fast mass transfer facilities from the interconnected hierarchically porous network of the diatomite structure.

The study of the adsorption mechanism indicates that the parent diatoms shows a physisorption process on a homogeneous surface, while; FeOOH/Di shows a chemisorption process on a heterogeneous adsorbent surface. Thermodynamic data indicate that the adsorption process is spontaneous, disordered and endothermic.

REFERENCES

Alomar, M. K.; Alsaadi, M.A.; Hayyan, M.; Aki, S.; Ibrahim, M. and Hashim, M. A. (2017). Allyl triphenylphosphonium bromide based DES-functionalized carbon nanotubes for the removal of mercury from water. *Chemosphere*, 167, 44-52. https://doi.org/10.1016/j..2016.09.133.

Atar, N. and Olgun, A. (2009). Removal of basic and acid dyes from aqueous solutions by a waste containing boron impurity. *Desalination*, 249, 109–115.

Atta, A. M.; Al-Lohedan, H. A.; Tawfik, A. M. and Ezzat, A. O. (2016). Application of Super-Amphiphilic Silica-Nanogel Composites for Fast Removal of Water Pollutants. *Molecules*, 21(10), 1392. https://doi.org:10.3390/molecules21101392

Chai, J-B.; Au, P-I.; Mubarak, N. M.; Khalid, M.; Ng, W. P-Q.; Jagadish, P.; Walvekar, R. and Abdullah, E. C. (2020). Adsorption of heavy metal from industrial wastewater onto low-cost Malaysian kaolin clay–based adsorbent. *Environmental Science and Pollution Research*, 27 (12), 13949–13962.

Choma, J. (2011). Application of Nanoporous Materials in Water Treatment. *Ochrona Środowiska.*, 33(4), 15-22.

Chua, Y. T.; Lin, C. C.; Kleitz, F. and Simon, S. (2015). Synthesis of mesoporous carbon–silica nanocomposite water-treatment membranes using a triconstituent co-assembly method. *Journal of Materials Chemistry A*, 3(19), 10480-10491.

Dąbrowski, A. (2001). Adsorption from theory to practice. *Advances in Colloid and Interface Science*, 93, 135-224.

De Castro Dantas, T. N., Dantas Neto, A. A., De A. Moura, M. C. P. (2001). Removal of chromium from aqueous solutions by diatomite treated with microemulsion. *Water Research*, 35 (9), 2219–2224.

Du, Y.; Zhen, S.; Wang, J.; Ma, Y.; Wu, J. and Dai, H. (2022). FeOOH-MnO2/Sepiolite and Fe2O3-MnO2/Diatomite: Highly efficient adsorbents for the removal of As(V). *Applied Clay Science*, 222, 106491

ElSayed, E. S. E. B. (2018). Natural diatomite as an effective adsorbent for heavy metals in water and wastewater treatment (a batch study). *Water Science*, 32, 32–43. https://doi.org/10.1016/j.wsj.2018.02.001

Faria, M. C. S.; Rosemberg, R. S.; Bomfeti, C. A.; Monteiro, D. S.; Barbosa, F.; Oliveira, L. C. A.; Rodriguez, M.; Pereira, M. C. and Rodrigues, J. L. (2014). Arsenic removal from contaminated water by ultrafine d-FeOOH adsorbents. *Chemical Engineering Journal*, 23, 47-54.

Faust, S. D. and Aly, O. M. (1987). Adsorption Process for Water Treatment. Butterworths Publishers, Stoneham. 508 pp.

Fernández-Luqueño, F.; López-Valdez, F.; Gamero-Melo, P.; Luna-Suárez, S.; Aguilera-González, E. N.; Martínez, A. I.; García-Guillermo, M. D. S.; Hernández-Martínez, G.; Herrera-Mendoza, R.; Álvarez-Garza, M. A. and Pérez-Velázquez, I. R. (2013). Heavy metal pollution in drinking water - a global risk for human health: A review. *African Journal of Environmental Science and Technology*, 7(7): 567-584.

Fu, D.; He, Z.; Su, S.; Xu, B.; Liu, Y. and Zhao, Y. (2017). Fabrication of a-FeOOH decorated graphene oxide-carbon nanotubes aerogel and its application in adsorption of arsenic species. *Journal of Colloid and Interface Science*, 505, 105–114.

Ghasemi, H.; Aghabarari, B.; Alizadeh, M.; Khanlarkhani, A. and Abu-Zahra, N. (2020). High efficiency decolorization of wastewater by Fenton catalyst: Magnetic iron-copper hybrid oxides. *Journal of Water Process Engineering*, 37, 101540.

Ghasemi, H.; Mozaffari, S.; Mousavi, S. H.; Aghabarari, B. and Abu-Zahra, N. (2021). Decolorization of wastewater by heterogeneous Fenton reaction using MnO2-Fe3O4/CuO hybrid catalysts. *Journal of Environmental Chemical Engineering*, 9 (2), 1.

Ghobara, M.; El-Sheekh, M.; Hamed, A.; Abdelhamid, M. and Pack, S. P. (2024). Diatom Nanostructured Biosilica. In: Abomohra, A., Ende, S. (eds) Value-added Products from Algae. Springer, Cham. https://doi.org/10.1007/978-3-031-42026-9_14.

Gusain, R.; Kumar, N. and SinhaRay, S. (2020). Recent advances in carbon nanomaterial-based adsorbents for water purification. 05091. *Coordination Chemistry Reviews*, 405, 213111.

Hakami, O.; Zhang, Y. and Banks, C. J. (2012). Thiol-functionalised mesoporous silicacoatedmagnetite nanoparticles for high efficiency removal and recovery of Hg from water. *Water Research*, 46, 3913-3922. https://doi.org/10.1016/j.watres.2012.04.032.

Hamed, A. (2023). A brief and general overview on diatoms and their applications: A review. *Egyptian Journal of Phycology*, 24, 1-53

Hao, Y. M.; Chen, M. and Hu, Z. B. (2010). Effective removal of Cu (II) ions from aqueous solution by amino-functionalized magnetic nanoparticles. *Journal of Hazardous Materials*, 184, 392–399.

Hasle, G. R. and Fryxell, G. A. (1970). Diatoms: Cleaning and Mounting for Light and Electron Microscopy. *Transactions of the American Microscopical Society*, 89, 469–474.

Homayoon, F.; Faghihian, H. and Torki, F. (2017). Application of a novel magnetic carbon nanotube adsorbent for removal of mercury from aqueous solutions. *Environmental Science and Pollution Research*, 24, 11764-11778.

Ilia, I. K.; Stamatakis, M. G. and Perraki, T. S. (2009). Mineralogy and technical properties of clayey diatomites from north and central Greece. *Central European Journal of Geosciences*, 1, 393–403 https://doi.org/10.2478/v10085-009-0034-3.

Jang, M.; Min, S.; Park, J. K. and Tlachac, E. J. (2007). Hydrous ferric oxide incorporated diatomite for remediation of arsenic contaminated groundwater. *Environmental Science & Technology*, 40, 1636-1643.

Jousé, A. P.; Mukhina, V. V. and Kozlova, O. G. (1969). Diatoms and Silicoflagellates in Bottom Sediments of the Pacific Ocean, in The Pacific Ocean, Microflora and Microfauna in Recent Sediments of the Pacific Ocean, Ed. by P. L. Bezrukov (Nauka, Moscow) 7, 7–47.

Kingston, C. (2003). Araphid and Monoraphid Diatoms, in: Freshwater Algae of North America, Edited by John D. Wehr and Robert G. Sheath. Elsevier Science (USA). 16, 559-636.

Knoerr, R.; Brendle, J.; Lebeau, B. and Demais, H. (2013). Preparation of ferric oxide modified diatomite and its application in the remediation of As(III) species from solution. *Microporous and Mesoporous Materials***,** 169, 15 185-191.

Koduru, J. R.; Karri, R. R. and Mubarak, N. M. (2019). Smart Materials, Magnetic Graphene Oxide-Based Nanocomposites for Sustainable Water Purification. In: Inamuddin, Thomas S., Kumar Mishra R., Asiri A. (eds) Sustainable Polymer Composites and Nanocomposites. Springer, Cham 759-781.

Lemessa, G.; Chebude, Y. and Alemayehu, E. (2023). Adsorptive removal of Cr (VI) from wastewater using magnetite–diatomite nanocomposite *AQUA - Water Infrastructure Ecosystems and Society*, 72(12), 2239. https://doi.10.2166/aqua.2023.132.

Lin, L. C.; Thirumavalavan, M. and Lee, J. F. (2015). Facile synthesis of thiol-functionalized mesoporous silica e their role for heavy metal removal efficiency. *Clean – Soil, Air, Water*, 43 (5), 775–785. https://doi.org/10.1002/clen.201400231.

Liu, X.; Sun, C.; Liu, H.; Tan, W. H.; Wang, W. and Snape, C. (2019). Developing hierarchically ultra-micro/mesoporous biocarbons for highly selective carbon dioxide adsorption. *Chemical Engineering Journal*, 361, 199-208.

Lowe, R. L. (2003). Keeled and Canalled Raphid Diatoms, in: Freshwater Algae of North America, Edited by John D. Wehr and Robert G. Sheath. Elsevier Science (USA). 19, 669-684.

Lu, Z.; Xu, X.; Chen, Y.; Wang, X.; Sun, L. and Zhuo, K. (2020). Nitrogen and sulfur co-doped graphene aerogel with hierarchically porous structure for high-performance supercapacitors. *Green Energy & Environment*, 5, 69-75.

Lucchini, M. A.; Testino, A.; Kambolis, A.; Proff, C. and Ludwig, C. (2016). Sintering and coking resistant core-shell microporous silica - nickel nanoparticles for CO methanation: towards advanced catalysts production. *Applied Catalysis B: Environmental*, 182, 94-101.

Luo, H.; Fu, F. and Tang, B. (2023). Ferrous sulfide supported on modified diatomite for the removal of Cr (VI): Performance and mechanism. *Colloids and Surfaces A: Physicochemical and Engineering* Aspects, 670, 131538.

Maia, L. F. O.; Hott, R. C.; Ladeira, P. C. C.; Batista, B. L.; Andrade, T. G.; Santos, M. S.; Faria, M. C. S.; Oliveira, L. C. A.; Monteiro, D. S.; Pereira, M. C. and Rodrigues, J. L. (2019). Simple synthesis and characterization of L-Cystinefunctionalizedd-FeOOH for highly efficient Hg(II) removal from contamined water and mining waste. *Chemosphere*, 215, 422-431.

Maity, J. and Ray, S. K. (2018). Chitosan based nano composite adsorbent—Synthesis, characterization and application for adsorption of binary mixtures of Pb(II) and Cd(II) from water. *Carbohydrate Polymers*, 182 159-171

Mashhadzadeh, H. A.; Fathalian, M.; Ghorbanzadeh, A. M. and Shahavi, M. H. (2018). DFT study of Ni, Cu, Cd and Ag heavy metal atom adsorption onto the surface of the zinc-oxide nanotube and zinc-oxide graphene-like structure. *Materials Chemistry and* Physics, 220, 366–373.

Moghaddam, S. T. and Naimi-Jamal, M. R. (2018). Reinforced magnetic polyurethane rigid (PUR) foam nanocomposites and investigation of thermal, mechanical, and sound absorption properties. *Journal of Thermoplastic Composite Materials*, 32 (9), 1224–1241.

Nenadovic, S.; Kljajevic, L.; Markovic, S.; Omerasevic, M.; Jovanovic, U.; Andric, V. and Vukanac, I. (2015). Natural Diatomite (Rudovci, Serbia) as Adsorbent for Removal Cs from Radioactive Waste Liquids. *Science of Sintering*, 47, 299-309.

Sharma, Y. C.; Srivastava, V.; Singh, V. K.; Kaul, S. N. and Weng, C. H. (2009). Nano-adsorbents for the removal of metallic pollutants from water and wastewater. *Environmental Technology*, 30 (6), 583–609.

Singh, D.; Verma, S.; Gautam, R. K. and Krishna, V. (2015). Copper adsorption onto synthesized nitrilotriacetic acid functionalized Fe_3O_4 nanoparticles: kinetic, equilibrium and thermodynamic studies. *Journal of Environmental Chemical Engineering*, 3, 2161–2171.

Song, J.; Cao, X. and Huang, Z. (2022). Diatomite-chitosan composite with abundant functional groups as efficient adsorbent for vanadium removal: Key influencing factors and influence of surface functional groups. *Journal of Molecular Liquids*, 367, 120428.

Srivastava, N. K. and Majumder, C. B. (2008). Novel biofiltration methods for the treatment of heavy metals from industrial wastewater *Journal of Hazardous Materials*, 151 (1), 1–8.

Taylor, J. C.; De La Rey, P. A. and Van Rensburg, L. (2005). Recommendations for the collection, preparation and enumeration of diatoms from riverine habitats for water quality monitoring in South Africa. *African Journal of Aquatic Science*, (1), 65-75.

Thakkar, M. and Mitra, S. (2017). Bimetallic Oxide Nanohybrid Synthesized from Diatom Frustules for the Removal of Selenium from Water. *Journal of Nanomaterials*, 1-9. https://doi.org/10.1155/2017/1734643

Todorciuc, T.; Bulgaria, L. and Pope, V. I. (2015). Adsorption of Cu (II) from aqueous solution on wheat straw Lignin: equilibrium and kinetic studies. *Cellulose Chemistry and Technology*, 49, 439–447.

Vakili, M.; Rafatullah, M.; Ibrahim, M. H.; Abdullah, A. Z.; Salamatinia, B. and Gholami, Z. (2014). Oil palm biomass as an adsorbent for heavy metals. *Reviews of Environmental Contamination and Toxicology*, 232, 61-88.

Valenzuela, F.; Quintana, G.; Briso, A.; Ide, V.; Basualto, C.; Gaete, J. and Montes, G. (2021). Cu(II), Cd(II), Pb(II) and As(V) adsorption from aqueous solutions using magnetic iron-modified calcium silicate hydrate: Adsorption kinetic analysis. *Journal of Water Process Engineering*, 40, 101951.

Vilbaste, S. (1994). The epiphytic and microphytobenthic diatoms in Estonian coastal waters (the Baltic Sea). In: Proceedings of the 13th International Diatom Symposium. D. Marino & M. Montresor (eds.). Biopress Limited, Bristol. 259-269.

Wang, Y.; Cai, J.; Jiang, Y.; Jiang, X. and Zhang, D. (2013). Preparation of biosilica structures from frustules of diatoms and their applications: Current state and perspectives. *Applied Microbiology and Biotechnology*, 97(2), 453–460**.**

Wang, Y.; Zhang, G.; Qiao, S. and Zhou, J. (2021) Magnetic Fe0/iron oxide-coated diatomite as a highly efficient adsorbent for recovering phosphorus from water. *Chemical Engineering Journal*, 412, 128696.

Wu, K.; Jing, C.; Zhang, J.; Liu, T.; Yang, S. and Wang, W. (2019). Magnetic Fe3O4@CuO nanocomposite assembled on graphene oxide sheets for the enhanced removal of arsenic(III/V) from water. *Applied Surface Science*, 466, 746-756.

Wolin, J. A. and Stone J. R. (2010). Diatoms as indicators of water level change in freshwater lakes. In: Stoermer EF and Smol JP (eds) The Diatoms: Applications for the Environmental and Earth Sciences. 2nd Edition.Cambridge: Cambridge University Press. 174–185.

Xie, S.; Wang, L.; Xu, Y.; Lin, D.; Sun, Y. and Zheng, S. (2020). Performance and mechanisms of immobilization remediation for Cd contaminated water and soil by hydroxy ferric combined acid-base modified sepiolite (HyFe/ABsep). *Science of The Total Environment*, 740, 140009.

Xiong, W. and Peng, J. (2008). Development and characterization of ferrihydrite-modified diatomite as a phosphorus adsorbent. *Water Research*, 42, 4869-4877.

Yadav, S. K.; Singh, D. K. and Sinha, S. (2014). Chemical carbonization of papaya seed orig-inated charcoals for sorption of Pb (II) from aqueous solution. *Journal of Environmental Chemical Engineering*, 2, 9–19.

Yadav, V. B.; Gadi, R. and Kalra, S. (2019). Clay based nanocomposites for removal of heavy metals from water: A review. *Journal of Environmental Management*, 232, 803–817.

Yang, F.; Zhang, S. S.; Li, H. P.; Li, S. S.; Cheng, K.; Li, J. S. and Tsang, D. C. W. (2018). Corn straw-derived biochar impregnated with α-FeOOH nanorods for highly effective copper removal. *Chemical Engineering Journal*, 348, 191–201. https:// doi.org/10.1016/j.cej.2018.04.161.

Yu, Y.; Zhuang, Y. Y. and Wang, Z. H. (2001). Adsorption of water-soluble dye onto functionalized resin. *Journal of Colloid and Interface Science*, 242, 288–293.

Zeng, Y.; Zeng, Z.; Ju, T. and Zhang, F. (2015). Adsorption performance and mechanism of perchloroethylene ona novel nano composite b-FeOOH-AC. *Microporous and Mesoporous Materials*, 210, 60-68.

Zhang, X.; Yao, H.; Lei, X.; Lian, Q.; Roy, A.; Doucet, D.; Yan, H.; Zappi, M. E. and Gang, D. D. (2021). A comparative study for phosphate adsorption on amorphous FeOOH and goethite (α-FeOOH): An investigation of relationship between the surface chemistry and structure. *Environmental Research*, 199, 111223.